Journal of Membrane Science 617 (2021) 118610

Contents lists available at ScienceDirect

Journal of Membrane Science

journal homepage: http://www.elsevier.com/locate/memsci

Upgrading polytetrafluoroethylene hollow-fiber membranes by CFD-optimized atomic layer deposition

Sen Xiong, Xiaojuan Jia, Kai Mi, Yong Wang *

State Key Laboratory of Materials-Oriented Chemical Engineering, College of Chemical Engineering, Nanjing Tech University, Nanjing, 211816, Jiangsu, PR China

ARTICLE INFO

Keywords:
Atomic layer deposition (ALD)
Computational fluid dynamics (CFD)
Hollow-fiber membranes
Polytetrafluoroethylene (PTFE)
Selectivity-permeability trade-off

ABSTRACT

Polytetrafluoroethylene hollow-fiber membranes (PTFE HFMs) with attractive advantages are highly promising for many applications, but strong hydrophobicity limits their uses in aqueous systems. To address this challenge, we propose to coat ultra-thin layers of alumina by atomic layer deposition (ALD) to upgrade performances of PTFE HFMs in water treatment. However, ALD usually requires time- and labor-consuming trial-and-error to optimize operating parameters. Herein, we use computational fluid dynamics (CFD) to identify most appropriate ALD parameters for PTFE HFMs functionalization. Following the CFD-optimized parameters, the ALD-treated membranes obtain significantly improved permselectivity and fouling resistance because of the remarkable increase in wettability at negligible cost in pore sizes. Impressively, water permeability of membranes is nearly doubled while rejection is increased by ~20%, which is seldom achieved by other methods. This CFD-optimized ALD process is expected to be a universal strategy to efficiently enhance the performances of polymeric membranes.

1. Introduction

With the merits of low cost, convenience, energy efficiency and environment friendliness, membrane separation is considered as one of the most promising solutions to settle the worldwide water scarcity [1–3]. Due to the superior physical and chemical stabilities, polytetrafluoroethylene (PTFE) is gaining interests to fabricate robust and flexible membranes. Nowadays, PTFE membranes have been widely utilized in gas purification, membrane distillation, oil/water separation and many other applications [4]. However, the low surface energy makes PTFE membranes strongly hydrophobic, which will lead to low water flux and severe membrane fouling in water treatment.

Surface modification, enabled by various methods including wet chemistry, plasma treatment, irradiation, surface coating, and so on [5–12], is frequently adopted to enhance the separation ability of PTFE membranes. However, wet chemistry, plasma treatment, and irradiation are enabled by breaking C–F bonds to generate oxygen-containing groups, which are destructive methods and may cause self-degradation of PTFE backbones. Moreover, these methods also have their own limitations. Wet chemistry modifications require harsh conditions to modify PTFE membranes. For example, a mixture solution of potassium permanganate and nitric acid is used to oxidize the PTFE membranes under heating conditions [5]. Such wet chemistry modifications are hard to operate and will produce highly corrosive and oxidative effluents. The plasma generated oxygen-containing groups are unstable, which are gradually decaying and the hydrophilicity will loss with the passage of time [7]. Surface coating is a physical functionalization method, the adhesion between coating layers and PTFE matrix is weak, which may cause progressive loss of coating layers during separation processes. Additionally, pore blocking in the modification processes may also occur, resulting in significant reduction of water permeance. Therefore, long-standing, efficient, and precisely controllable functionalization for PTFE membranes is still challenging and highly demanding.

Atomic layer deposition (ALD) is an advanced gas-phase deposition technology and has been introduced into the membrane functionalization in last decade [13]. Due to the self-limiting nature of ALD, the thickness and composition of deposited layers can be tuned at atomic level [14]. By using highly reactive precursors, ALD can deposit uniform, conformal and high-quality films on almost any substrates under mild reaction conditions, which makes it particularly suitable for the functionalization of polymeric membranes with low surface energy [13, 15–21]. In previous works, we have demonstrated that various polymeric membranes can be easily modified by ALD to upgrade separation performances [22–25]. Xu et al. used ALD to deposit Al_2O_3 on PTFE

* Corresponding author.
E-mail address: yongwang@njtech.edu.cn (Y. Wang).

https://doi.org/10.1016/j.memsci.2020.118610
Received 24 July 2020; Received in revised form 4 August 2020; Accepted 6 August 2020
Available online 22 August 2020

flat-sheet membranes and significantly enhanced the separation performances [22]. Due to the low surface energy of PTFE, Al_2O_3 underwent subsurface nucleation, which guaranteed strong adhesion between Al_2O_3 layers and PTFE matrices. After totally covered by Al_2O_3, PTFE membranes exhibited simultaneously increased selectivity and permeability. Wang et al. deposited conformal and uniform TiO_2 layers on the polyvinylidene fluoride (PVDF) membranes through ALD [24]. In addition to the significant promotion of separation performances, thermal stability of PVDF membranes was also enhanced because of the shielding effect from the deposited TiO_2 layers.

Comparing with flat-sheet membranes, hollow-fiber membranes (HFMs) have gained increasing attention due to larger surface area and higher package density [26]. The operation costs and life span of HFMs are appreciably affected by surface properties, while the complex structures make them hard to be modified with common methods. Therefore, efficient functionalization on HFMs is more urgently needed. Jia et al. used ALD to improve the surface property of polypropylene (PP) HFMs and confirmed that ALD could functionalize porous HFMs efficiently. With certain deposition cycles of Al_2O_3, the water flux, selectivity and fouling resistance of PP HFMs were increased [27]. However, currently used ALD setups and strategies are mostly designed for microelectronic industries. Utilizing ALD to functionalize membranes requires cumbersome trial-and-error to identify the appropriate reaction pressure, precursor distribution, and other parameters [28,29]. More importantly, ALD is a delicate process and highly sensitive to substrates, therefore, many depositing parameters and deposition behavior on different substrates are unique. Reported results of ALD on other membranes cannot be directly applied to PTFE HFMs which we investigated here. That is, ALD parameters on other substrates can be referred, while considerable trial experiments for ALD on specific membranes are still required. Consequently, there is a strong need to streamline the application of ALD in modification and functionalization of membranes.

Computational fluid dynamics (CFD) simulation is a discrete numerical method using computers to quantitatively describe the solution of flow field in time and space. By introducing CFD into ALD processes, the reaction temperature, operation pressure, precursor concentration and other parameters can be optimized through simulations, which provide great convenience to guide the practical ALD experiments [30–32]. Yuan et al. used CFD to study the influence of exposure time, reactor structure and deposition temperature on the Al_2O_3 ALD process [30]. Simulation results showed that extended exposure time, higher reaction temperature, and top-inlet chamber structure were advantageous for depositing uniform Al_2O_3 layers. By combining the details of fluid flow and surface reactions, they further confirmed the self-limiting nature of ALD processes. The calculated growth rate agreed with experimental results very well [31]. Chen et al. used CFD to analyze the effects of temperature, precursor mass fraction, mass flow, and reaction pressure on the process of Al_2O_3 depositing on silicon wafers [32]. Under certain temperature and mass flow rate, lower reaction pressure and higher precursor mass fraction could facilitate the uniform ALD deposition. However, these works were concentrated on simulations or just conducted on simple substrates (plane wafers), few works used simulation results to directly guide practical ALD processes, and there is no report on CFD-guided ALD for separation membranes.

To alleviate the burdensome experimental optimization efforts, we use CFD to simulate the ALD of Al_2O_3 on PTFE HFMs. Al_2O_3 is one of the most widely studied models and the high reactivity precursor makes Al_2O_3 can be deposited on any possible substrates. Moreover, the Al_2O_3 surface will be hydroxylated under aqueous condition while its bulk volume keeps stable [13,33], which is particularly suitable for polymer membranes used in water treatments. With guidance of CFD results, the optimal ALD parameters are successfully determined. By following CFD-identified parameters, the selectivity, permeability and fouling resistance of PTFE HFMs are significantly enhanced after ALD functionalization. This work demonstrates that CFD can greatly facilitate the application of ALD in PTFE hollow-fiber membrane functionalization, and we expect this CFD-optimized ALD strategy would also be efficient in improving performances of other membranes.

2. CFD simulation details

2.1. ALD setup and processes

The ALD setup (Savannah S100, Cambridge NanoTech) is composed of precursor cylinders, nitrogen supply devices, vacuum systems, reaction chamber, and computer control systems. These five main parts are connected by pipes and valves (Fig. 1a). The actual size of reaction chamber is shown in Fig. 1b. A typical ALD process includes four steps. Firstly, excessive precursor ***A*** is pulsed into the reaction chamber to react with substrates. Secondly, high purity nitrogen is pulsed to sweep unreacted precursors and by-products out of the reaction chamber. Thirdly, the precursor ***B*** is pulsed into reaction chamber to react with the adsorbed precursor ***A***. Finally, another purge step is conducted to clean the reaction chamber for next ALD cycle. By controlling the number of ALD cycles, the thickness of deposition layer can be precisely tuned. In this work, trimethylaluminium (TMA) and deionized (DI) water are used as precursors to deposit Al_2O_3. The mass changing of solid species O<s> ($ng/cm^2 \cdot s$) on the substrate during TMA pulse step is used as reference of deposition rate [32].

2.2. Simulation model and boundary conditions

The simulated reaction chamber is constructed based on the size of actual ALD chamber. The bottom part of reaction chamber is defined as the xy-plane and the chamber center is the origin point of the simulation system. The inlet and outlet are in the negative and positive direction of x-axis, respectively (Fig. 2). To meet the high-accuracy requirement, the reaction chamber model is divided into 92,407 grids. The gas flow rate and reaction temperature is set to 20 sccm and 373 K (100 °C), respectively. The reaction pressure ranges from 0.2 to 50 torr during the simulation. The mass fraction and pulsing order of precursors are set by the user define function. A no-slip boundary condition and heat insulation wall are assumed. The residuals for continuity and other parameters are 10^{-5} and 10^{-6}, respectively.

In simulation processes, the ALD is conducted with the "pulse-purge" mode, the time required to sweep all precursor molecules and by-products out reaction chamber is the minimum purge time. The gas flow in ALD setup is laminar flow during the deposition process [34]. The Arrhenius expression is used to describe chemical kinetics of reactions between precursors and surface species. To calculate the momentum, mass, and energy transports in the simulation process, the general flow field equations with tensor form are given [35]:

$$\frac{\partial}{\partial t}(\rho \vec{V}) + \nabla \cdot (\rho \vec{V} \vec{V}) = -\nabla P + \nabla \cdot \bar{\bar{\tau}} + \rho \vec{g} + \vec{F} \tag{1}$$

$$\bar{\bar{\tau}} = \mu \left[\left(\nabla \vec{V} + \nabla \vec{V}^T \right) - \frac{2}{3} \nabla \cdot \nabla \vec{V} I \right] \tag{2}$$

$$\frac{\partial}{\partial t}(\rho E) + \nabla (\vec{V}(\rho E + P)) = \nabla \left(k \nabla T - \sum h \vec{J} + (\bar{\bar{\tau}} \vec{V}) \right) + S_h \tag{3}$$

$$\frac{\partial}{\partial t}(\rho Y_i) + \nabla (\rho \vec{V} Y_i) = -\nabla \cdot \vec{J}_i + R_i + S_i \tag{4}$$

$$\vec{J}_i = -\rho D_{m,i} \nabla Y_i - D_{T,i} \frac{\nabla T}{T} \tag{5}$$

where ρ and $\vec{V}$ are density and velocity of the gas mixture, respectively. P is the static pressure, $\bar{\bar{\tau}}$ is the stress tensor, $\vec{g}$ is the component of gravity on the fluid flow direction, $\vec{F}$ is the external body force, μ is the fluid dynamic viscosity, T is the temperature, I is unit tensor, E is the

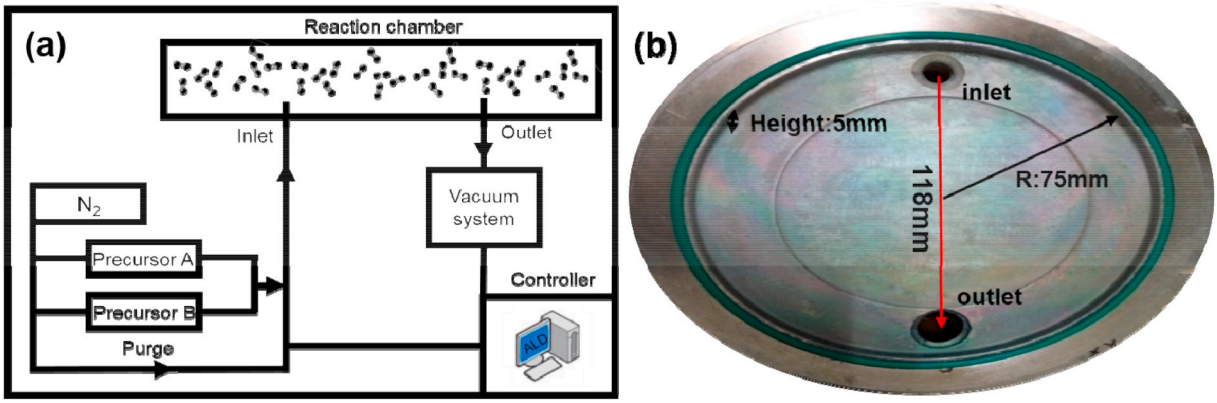

Fig. 1. (a) Diagram of the ALD setup; (b) digital image of the actual ALD reaction chamber.

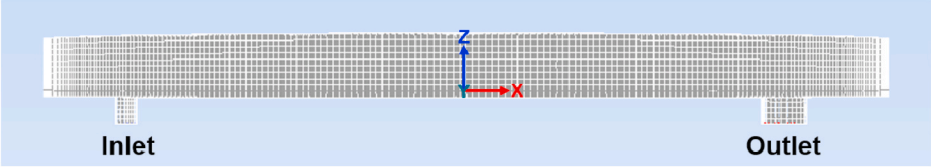

Fig. 2. Diagram of the simulated reaction chamber.

internal energy of the fluid, R_i, S_i, $\vec{J}_i$, $D_{m,i}$ and $D_{T,i}$ represent the reaction terms, mass transfer source terms, diffusive flux, mass diffusivity and heat diffusivity of specie i, respectively. S_h is the heat transfer source term.

3. Experimental

3.1. Materials

PTFE HFMs (outer diameter: 1.7 mm, wall thickness: 350 μm, mean pore size: 200 nm) were purchased from Zhejiang DongDa Water Industry Co., Ltd. TMA with purity of 99.99% and DI water were obtained from Nanjing University and Wahaha Co., Ltd., respectively. Ultrahigh purity N_2 (99.99%, Tianhong Gas Company) was applied in the ALD setup for precursor transportation and purgation. Ethanol (99.7%, Yasheng Chemical Co., Ltd.) was used as cleaning agent. Monodisperse solution of 22-nm SiO_2 microspheres was obtained from Aladdin chemicals. Bovine serum albumin (BSA, M_w = 67 kDa, 97%) was purchased from GM corporation and used as model pollutant to test the fouling resistance of pristine and functionalized membranes. CAS numbers of all used chemicals were listed in Table S1.

3.2. ALD of Al_2O_3 on PTFE hollow-fiber membranes

All PTFE HFMs were cut into 8 cm and successively washed with ethanol and DI water, then dried at 60 °C. The ALD setup was preheated to 100 °C before deposition. The totally dried membranes were put into reaction chamber and stored under vacuum for 30 min to remove adsorbed air or water molecules. Considering the high saturated vapor pressures of TMA and water, shorter exposure times are chosen to guarantee the appropriate pressure in reaction chamber. As shown in Fig. S1, the simulation result shows that the reaction between TMA and membrane surface is fast and reaches equilibration within 0.01 s. However, considering the complex structure of PTFE HFMs, the exposure time is extended to 5 s to facilitate the diffusion of precursors into membranes. Taken together, the pulse/exposure/purge times for TMA and DI water were 0.05 s/5 s/30 s and 0.03 s/5 s/30 s, respectively. Three Si wafers were placed near membranes in the reaction chamber as reference to record the growth rate of Al_2O_3 films. Under selected ALD parameters, the growth rate of Al_2O_3 films was 1.1 Å/cycle (Fig. S2), therefore, the pore size reduction of the membranes was about 2.2 Å/cycle. Different deposition cycles up to 500 were conducted to study the influence of ALD processes on PTFE HFMs.

3.3. Characterization

Morphologies of pristine and functionalized PTFE HFMs were observed by the field emission scanning electron microscope (FESEM, Hitachi S4800) operated at 5 kV. The distribution of Al element in membranes was detected by the energy dispersive X-ray spectrometer (EDS, EMAX X-act). The growth rate of Al_2O_3 films deposited on Si wafers was determined by a spectroscopic ellipsometer (Complete EASEM-2000U, J. A. Woollam) with an incidence angle of 70°. Contact angle meter (DropmeterA-100, Maist) was employed to test the wetting behavior of PTFE HFMs before and after deposition. Every sample was tested at least 5 times and the average value was recorded. Inductively coupled plasma-optical emission spectrometry (ICP-OES, Optima 7000DV, PerkinElmer) was used to test the concentration of 22-nm SiO_2 microspheres in feed and filtration solutions. The concentration of BSA solution was measured by ultraviolet–visible spectrometer (UV, NanoDrop 2000C, Thermo) at 280 nm. The thermal analyzer (TG209F1, Netzsch) was employed to conduct thermogravimetric analysis (TGA) of PTFE HFMs. All samples were heated under O_2 atmosphere from 20 °C to 700 °C with a heating rate of 10 °C/min.

3.4. Filtration tests

The separation performance of pristine and deposited PTFE HFMs was tested in a homemade apparatus under room temperature. Tested membranes were cut into certain length and sealed in hoses by epoxy resin. Then the hose was connected to the apparatus and pre-run for 10 min under 1 bar to achieve stable pure water permeance (PWP, L/m^2·h·bar). To alleviate the influence of strong hydrophobicity, pristine PTFE membranes were wetted by ethanol before test. The *PWP* was calculated by Eq. (6):

$$PWP = \frac{Q}{A\Delta Pt} \quad (6)$$

where Q (L) was the water flux, A (m^2) was the effective filtration area, ΔP (bar) was the operation pressure, and t (h) was the testing time.

22-nm SiO_2 microspheres solution was used to test the separation performance after PWP measurement. The concentration of 22-nm SiO_2 microspheres in feed and permeation was investigated by ICP-OES. The rejection of SiO_2 microspheres was calculated by Eq. (7):

$$R = \left(1 - C_p / C_f\right) \times 100\% \quad (7)$$

where C_f and C_p (g/L) were the concentration of 22-nm SiO_2 microspheres in feed and permeation, respectively.

3.5. Fouling resistance tests

0.5 g BSA was dissolved in 1 L phosphate buffer solution (pH = 7) to prepare BSA test solution. Tested membranes were immersed in 7 mL BSA solution under 25 °C for 12 h. The initial and final concentrations of BSA solution were measured by UV spectrometer. The surface adsorption capacity M (μg/cm^2) was calculated by Eq. (8):

$$M = V\left(C_i - C_f\right)/A \quad (8)$$

where V (L) was the volume of BSA solution, A (cm^2) was the effective membrane area, C_i and C_f (g/L) were the initial and final concentrations of the BSA solution, respectively.

4. CFD simulation results

4.1. The influence of reaction pressures

Due to the self-limiting property and existence of ALD window [14], the precursor dosage and reaction temperature show negligible influence on the optimization of ALD processes. On the contrary, the reaction pressures can be varied in a broad range and influence the fluid flow in reaction chamber, which is an important parameter in ALD processes. Moreover, the reaction pressure is highly associated with precursor pulse processes, thus we choose the reaction pressure as research object. Under different reaction pressures, the O<s> on substrate shows distinct changing rates, which indicates different deposition rates of the simulated ALD process (Fig. 3). The deposition rate increases with reaction pressures and shows position-independent homogeneity under lower pressures (<10 torr). After the pressure reaches 10 torr, the deposition rate is gradually deviating from the homogeneous deposition of O<s> (the inset in Fig. 3). The deposition rate around the origin is slightly slower than that at the inlet and outlet directions. With further increasing reaction pressure (50 torr), we can observe more pronounced inhomogeneous deposition rates. The rate value around the outlet is slightly higher than that at inlet direction. Notably, the rate around origin under 50 torr is even slower than that under 10 torr. In order to get higher pressure, more carrier gas is inflated into reaction chamber during the pulse step, which will cause severe precursor overdosage and pronounced fluid disturbance in reaction chamber. Moreover, the forced inflation and deflation procedures will strengthen the collision between precursor molecules and substrates. As a result, these factors worsen the inhomogeneous deposition of ALD processes [32]. Higher reaction pressure not only causes inhomogeneous deposition on substrates, but also exacerbates the waste of precursors. Due to the self-limiting property of ALD, once the adsorption on substrate surface is saturated, overdosed precursors are swept out reaction chamber and wasted. Therefore, to guarantee the homogeneous deposition and save expensive precursors, we choose 0.2 torr as the reaction pressure for further simulation.

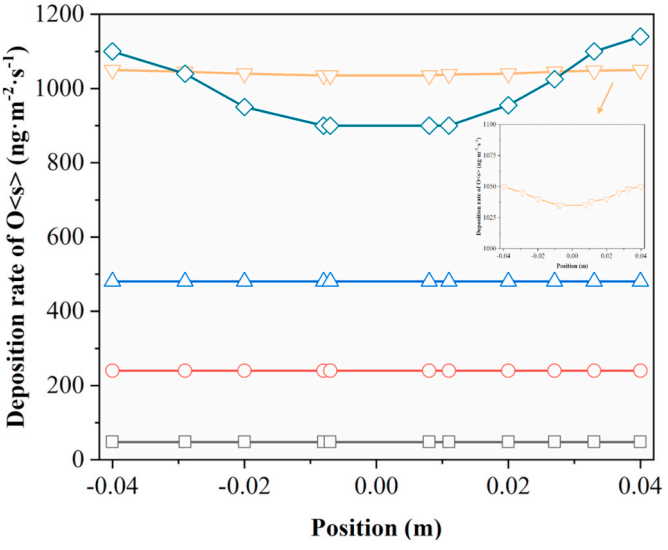

Fig. 3. Simulation results of O<s> changing rate under different pressures. The inset is the local enlarged diagram of O<s> under 10 torr.

4.2. Fluid velocity distribution in reaction chamber

To investigate the fluid flow status in reaction chamber, we analyzed the fluid velocity distribution at the height of 3 mm under 0.2 torr. As shown in Fig. 4a, due to the forced inflation and deflation processes, the disturbance is inevitable at inlet and outlet. Interestingly, the velocity at outlet is faster than that at the inlet. With the increasing of reaction pressure, more volume of N_2 is inflated in and deflated out the reaction chamber within designed time, which will cause intense disturbance. Nevertheless, the inhomogeneity of deposition rate appears at 10 torr and is getting worse under 50 torr, demonstrating the disturbance can hamper the uniform deposition of ALD processes under certain level. With the development of fluid flow, an hourglass-shaped area is formed between the inlet and outlet. Although the rate is slower in this area, the distribution of velocity is uniform and has no obvious fluctuation. Except for these two areas, velocity at other area in chamber is affected by the boundary and approaches to zero. Unlike the varying velocity in the chamber, the fluid flow has negligible effect on static pressure (Fig. 4b). Combining these two results with the influence of reaction pressures, we can conclude that the pulse and purge steps will disturb the fluid flow and the distribution of precursors with increasing reaction pressure. However, the static pressure is uniform throughout the reaction chamber at lower reaction pressure, which maintains the free diffusion of precursor molecules and guarantees the uniform deposition of ALD.

4.3. Influence of active site density

PTFE is a chemical inert material, which means that there are few active sites on its surface and majority ALD processes may occur at the chain defects and chain termini [36]. To explore whether the Al_2O_3 can be uniformly deposited on the PTFE under selected parameters, we simulated the ALD process on substrates with different active site densities (1×10^{-9}–2×10^{-8}). As shown in Fig. 5, the mass changing is consistent with experiments [37] and a remarkably high deposition rate can be observed on the surface with denser active sites. The main procedure of ALD processes is the rapid reaction between precursors and surface active sites, therefore, the reaction rate is directly influenced by the number of active sites. While the Al_2O_3 can also be deposited on the active site scarce substrates with slower and uniform deposition rate. This result matches well with experimental results and explains the growth rate difference of ALD on various polymers [23,38–40]. For activated polymeric membranes (such as plasma treated or polyphenol sensitized), the active site density on membrane surface is significantly

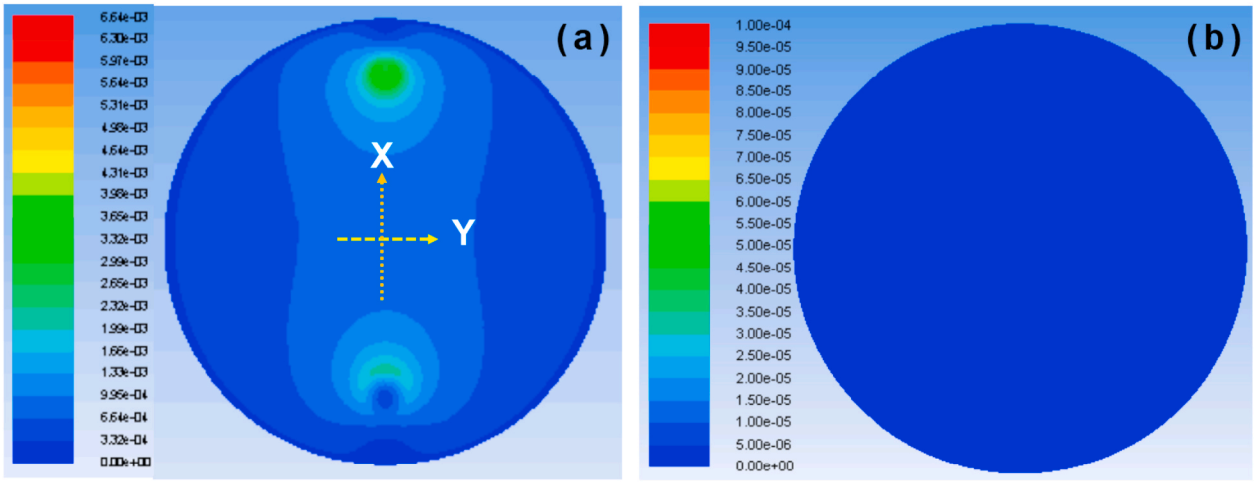

Fig. 4. Simulation results of (a) fluid flow velocity and (b) static pressure distribution at the height of 3 mm under 0.2 torr in reaction chamber.

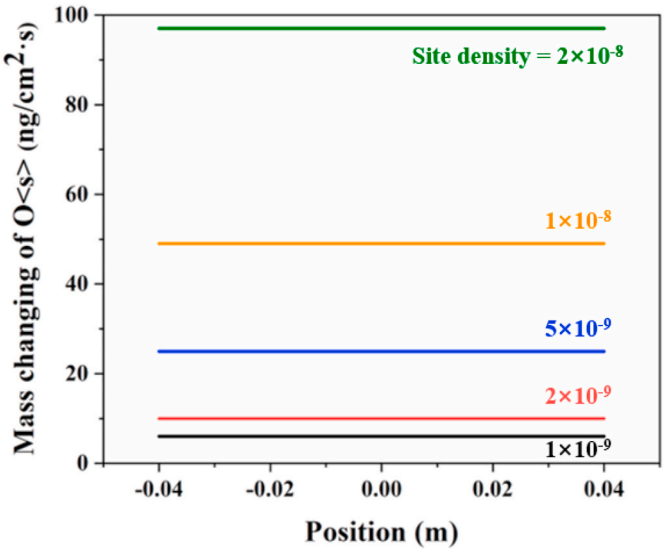

Fig. 5. Surface deposition rate of O<s> with different active site densities.

increased. More precursors can be adsorbed on membrane surface by the functional groups at initial stage, which endows the ALD process with a high and constant growth rate at beginning stage and avoids the subsurface nucleation [39,40]. On the untreated polymeric membranes, the deposition rate was changing with ALD cycle numbers. At initial stage, precursors should diffuse into subsurface region to nucleate, thus the deposition rate is the slowest during the deposition process. With increasing ALD cycles, the nuclei come out to the surface with granular structures, which provide large number of active sites and significantly accelerate the deposition rate. After forming intact layers, the shrinkage of surface area leads to a slower but constant deposition rate [23]. The simulation result evidences that the active site density has significant impact on the deposition rate.

The deposition location in reaction chamber for PTFE HFMs is also optimized by CFD simulation. According to reaction pressure and velocity distribution simulation results, membranes are placed at the middle of the reaction chamber and perpendicular to the x-axis (the diagram is shown in Fig. 6a). The reaction temperature and pressure are 100 °C and 0.2 torr, respectively. As shown in Fig. 6b, the Al_2O_3 growth rate on different membranes is close to each other. Therefore, we believe that the ALD can deposit uniform Al_2O_3 layers on PTFE HFMs by using the CFD optimized operation parameters. Based on the simulation results, we find that reaction pressure, fluid flow and active site density have obvious impacts on the ALD processes. Increasing reaction pressure will promote the deposition rate, but higher pressures (≥10 torr) lead to

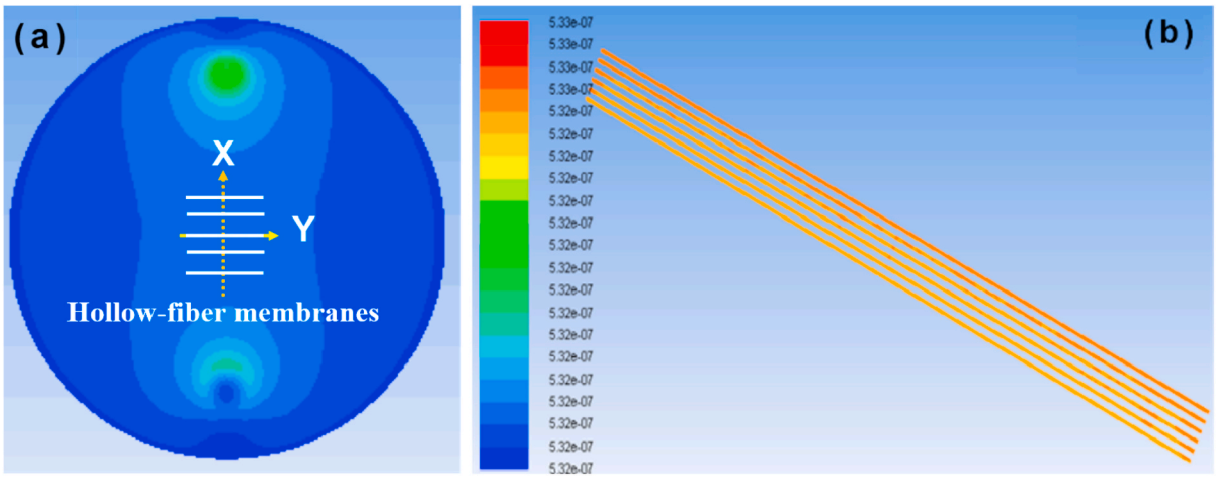

Fig. 6. (a) Diagram of PTFE HFMs setting position during the simulation; (b) simulation result of the Al_2O_3 deposition rate on the PTFE HFMs.

inhomogeneous deposition. To ensure lower pressure (0.2 torr) in the reaction chamber, we choose 0.05 s and 0.03 s as pulsing times for TMA and DI water, respectively. Although the reaction between TMA and membrane surface is very fast, precursor molecules still need time to diffuse through the membranes. Considering the complex structure of PTFE HFMs, the exposure time is set to 5 s in the experimental section.

5. ALD-functionalized PTFE hollow-fiber membranes

5.1. Evolution of surface morphology

After CFD simulation, PTFE HFMs are deposited under optimized parameters with different ALD cycles. Pristine membrane fibrils are stretched and some cracks can be observed on their surfaces (Fig. 7a) [41]. After deposited with 50 cycles of Al_2O_3, the crack width resembles increased (Fig. 7b). This phenomenon is caused by the nucleation growth of Al_2O_3 on the PTFE fibrils [42]. As illustrated above, the precursors diffuse into the subsurface region of PTFE membranes and start nucleation. Then the nuclei grow into discrete particulates on the fibril surface and form new "cracks". With rising ALD cycles, Al_2O_3 particulates continue to grow and connect each other (Fig. 7c–d). Finally, PTFE membranes are completely covered by intact ALD-deposited Al_2O_3 layers (Fig. 7e). With more ALD cycles, the pore size of PTFE HFMs is further reduced, which will significantly enhance the selectivity of membranes.

EDS is employed to observe the distribution of Al element in membranes after deposition. As shown in Fig. 8a, after 200 cycles of deposition, the Al element can be found throughout the membrane cross section, revealing that precursors can diffuse into the membrane and complete the ALD deposition. However, there is a content difference of Al element between the outer and inner surfaces (Fig. 8b–c). According to simulation results, the movement of precursor molecules is free diffusion and there is no additional driven force for precursor molecules penetrating into membranes. Moreover, the already formed Al_2O_3 layers on outer surface will reduce the pore size and increase entrance resistance. Therefore, the precursor molecules form concentration gradient in membrane pores, which leads to the content difference of Al element [43]. For the whole PTFE membrane functionalization process, the concentration difference will lead to gradient pore structures. The smaller pores on outer surface can promote the selectivity, and the larger pores inside can reduce the filtration resistance, thus the separation performance of PTFE HFMs can be enhanced by this gradient structure [44].

5.2. ALD growth mode and deposition mass on PTFE HFMs

According to surface active site density, there are two ALD growth modes. For active site abundant polymers, the growth rate of ALD processes is a constant value under different ALD cycles. For chemical inert polymers, the growth rate will undergo slow-fast-constant stages [23]. These two modes make ALD competent to deposit on any kind of polymers. To further confirm the growth mode and deposition amount of Al_2O_3 on PTFE HFMs, TGA is used to monitor the mass changes of deposited membranes. As shown in Fig. 9, the pristine membrane starts decomposing at 500 °C. The residual mass of pristine membrane approaches to zero at 700 °C, which means pristine membranes decompose completely at that temperature. After 100 and 300 cycles of ALD deposition, the starting and finishing points of decomposition are similar to pristine membranes. However, the residual masses of membranes deposited by 100 and 300 cycles are 1.9% and 9.1%, respectively. Although the deposition cycle increases 200% (from 100 to 300), the mass of deposited Al_2O_3 increases ~380% (from 1.9% to 9.1%). After 100 cycles deposition, Al_2O_3 clusters break through the subsurface region and provide active sites for further deposition, which significantly accelerate the growth rate [37]. This result confirms the existence of subsurface nucleation growth mode and is consistent with the observation above.

5.3. Wetting behavior changes

Hydrophilicity is an important physical property and has significant impact on the productivity of water treatment membranes [45]. As shown in Fig. 10, pristine membranes exhibit strong hydrophobicity with WCA of ~118°. At initial stage of ALD functionalization processes, the promotion of surface hydrophilicity is not pronounced. After 100 cycles of deposition, the WCA of deposited membranes is still higher than 100°. As confirmed by SEM images and TGA data, the mass fraction of Al_2O_3 is just 1.9 wt% and Al_2O_3 has not fully grown on the membrane surface under 100 cycles. With further increasing ALD cycles, the original surface is gradually covered by hydrophilic Al_2O_3, thus the membrane turns into hydrophilic and its WCA decreases to ~85° after 200 cycles of deposition. The WCA of deposited membranes is further reduced to ~35° after 400 cycles of deposition. These results show that ALD can effectively improve the water affinity of PTFE HFMs by depositing hydrophilic Al_2O_3 on membrane fibrils. Although the hydrophilicity is enhanced with more ALD cycles, the comprehensive influence of pore size reduction and hydrophilization on separation

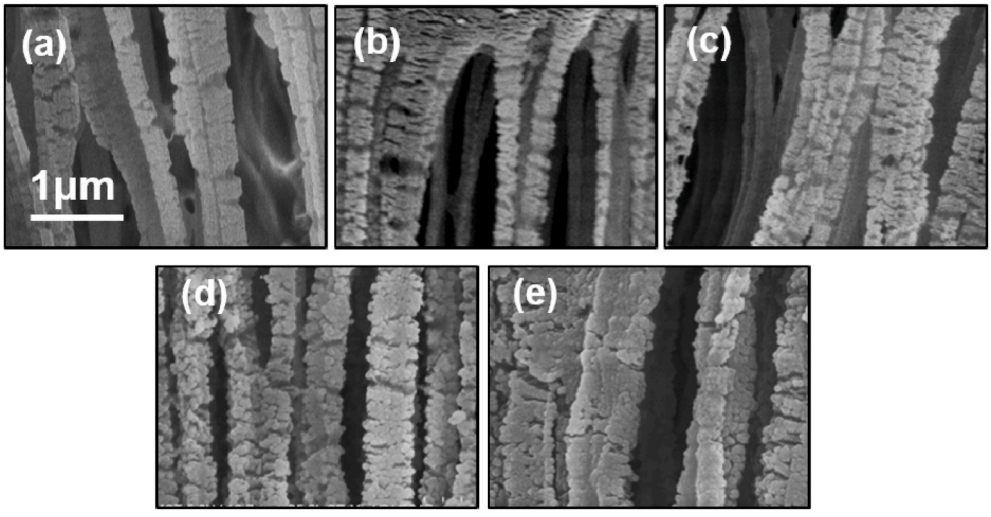

Fig. 7. Outer surface SEM images of (a) pristine membrane and membranes deposited with (b) 50, (c) 100, (d) 200 and (e) 300 ALD cycles. All images have the same scale bar as shown in (a).

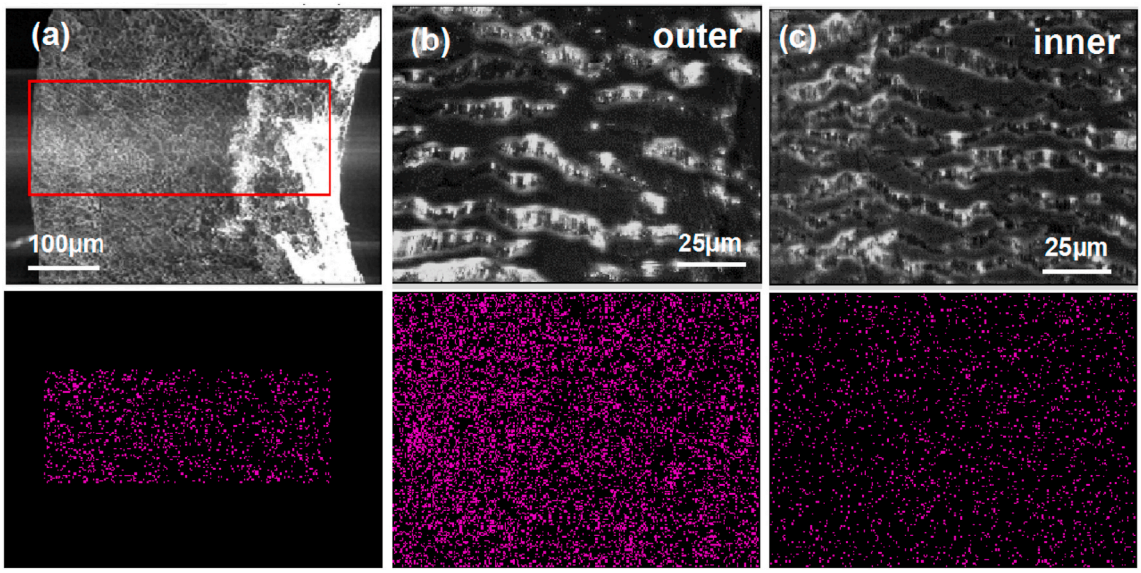

Fig. 8. SEM images (up) and EDS mapping (down) of 200-cycle-deposited membranes: (a) cross section, (b) outer surface, and (c) inner surface.

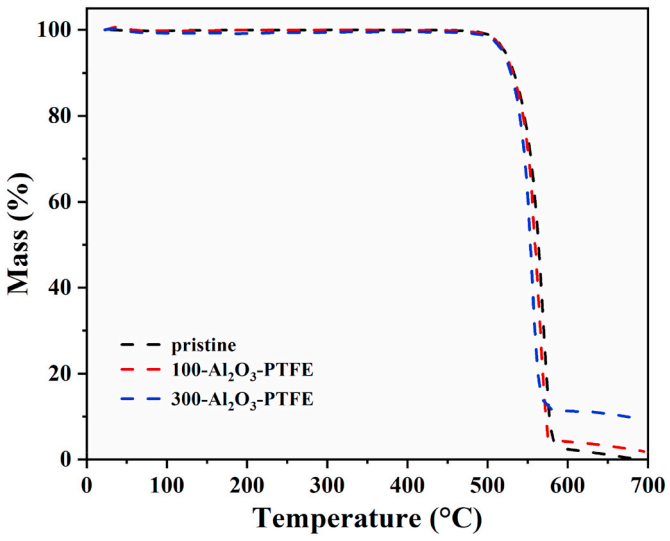

Fig. 9. TGA curves of pristine and PTFE HFMs deposited with different ALD cycles.

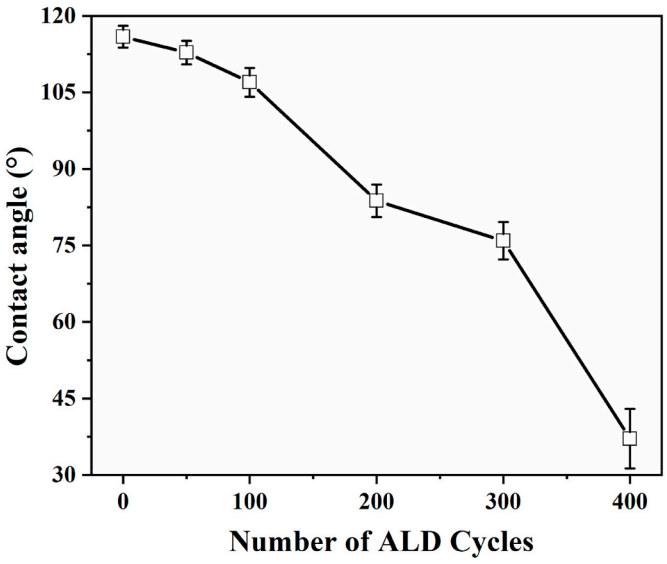

Fig. 10. WCAs of PTFE HFMs with different ALD deposition cycles.

performance should be taken into consideration. Therefore, further investigation is needed to determine the optimal number of deposition cycles.

5.4. Separation performances of functionalized PTFE HFMs

The most attractive advantage of ALD in membrane functionalization is the ability to break trade-off effect between selectivity and permeability [46]. In order to find optimal ALD cycles, pure water and 22-nm SiO_2 microspheres solution are used to examine the separation performance. As shown in Fig. 11, the PWP and rejection towards 22-nm SiO_2 microspheres of pristine membranes are ~96 L/(m^2 h bar) and ~77.1%, respectively. With more ALD cycles, the rejection keeps increasing and finally exceeds 95%. In contrast, the PWP increases first and then decreases under different ALD cycles. After 100 cycles of Al_2O_3 deposition, the PWP of PTFE HFMs reaches the maximum value of ~188 L/(m^2 h bar). This phenomenon seems inconsistent with previous observation in the WCA test and there are two possible reasons. Firstly, the WCA measurement is conducted under atmospheric pressure, no additional driven force acts on water droplets except for the gravity. Although the WCA exhibits a small decline after 100 cycles of deposition, there are many hydrophilic Al_2O_3 particulates on membrane fibrils (as shown in SEM images), which will reduce the threshold pressure during the filtration processes and facilitate water permeation [47]. Secondly, the permeability of membrane is a comprehensive outcome of surface property and pore size. When the surface is fully covered by metal oxide, the hydrophilicity of the membrane reaches maximum value and then keeps unchanged. On the contrast, the pore size will keep decreasing and increases mass transfer resistance, thus the PWP begins to decrease with more ALD cycles. Comparing with pristine membranes, the PWP and rejection of 100-cycle-deposited PTFE HFMs are significantly and simultaneously increased to 188 L/(m^2 h bar) and 93.4%, respectively. Combining with the TGA result, only 1.9 wt% of Al_2O_3 can greatly promote the separation performance of PTFE HFMs, which confirms that the ALD is highly effective for membrane functionalization.

The separation performance of ALD functionalized PTFE HFMs has been compared with the results of other modified membranes

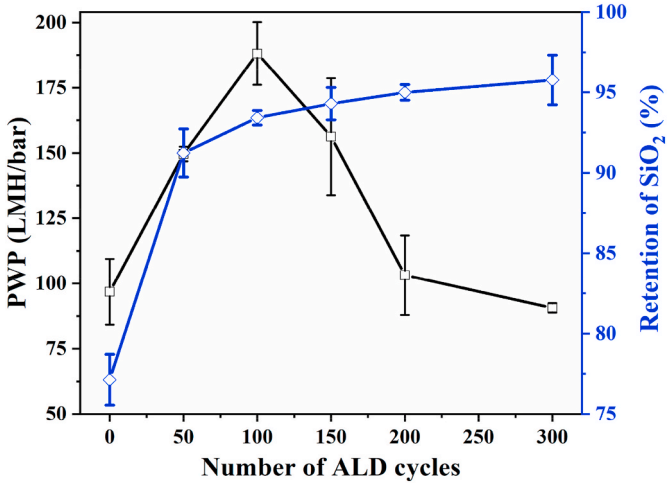

Fig. 11. Pure water permeance and SiO_2 microspheres retention of the pristine and Al_2O_3-deposited PTFE HFMs.

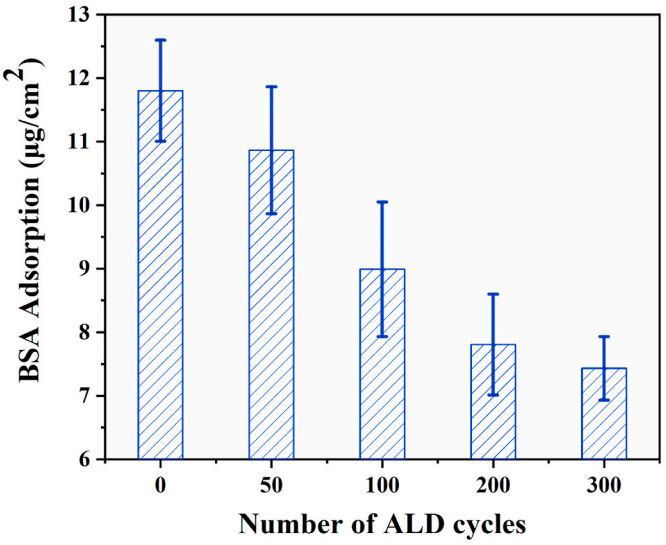

Fig. 12. Static adsorption test of pristine and Al_2O_3-deposited PTFE HFMs.

(Table S2). However, the promotions of flux and rejection are affected by many factors, including functionalization methods, type of pristine membranes, membrane pore sizes, and test conditions. For example, ALD functionalization has been conducted on the PP HFMs, PTFE HFMs, and PTFE flat-sheet membranes. Although these membranes have same pore size (0.2 μm), the separation performance promotions of these membranes are quite different. Therefore, the promotions of functionalized membranes tested under different variables are hard to compare with each other. It is worth noting that the ALD strategy is one of the most powerful methods to upgrade polymeric membranes. Firstly, the functionalization of membranes can be accomplished in a very short time. In this work, the PTFE HFMs are upgraded within only 2 h. Secondly, the polymeric membranes can be functionalized by ALD without any pretreatments. Thirdly, the ALD is a vapor phase deposition method, which has no risk of pore blocking during the membrane functionalization processes.

5.5. Fouling resistance changes of PTFE HFMs

Due to the large packing density of hollow-fiber membranes, the membrane fouling will dramatically increase the operational costs and decrease the service life of membrane modules [48]. Therefore, enhancing the fouling resistance is an effective way to further promote the practicality of hollow-fiber membranes. With the increase of hydrophilicity, the resistance of PTFE HFMs towards hydrophobic pollutants is also enhanced. As shown in Fig. 12, the adsorption capacity of pristine membranes towards BSA is ~12 μg/cm^2. After Al_2O_3 deposition, the adsorption capacity towards BSA is falling down. Specifically, the adsorption capacity shows a significant decrease of ~25% after 100 cycles of deposition. The value is further decreased to ~37.5% for the 300-cycle-deposited membranes. After coated with Al_2O_3, the hydrophilic metal oxide will attract more water molecules on membrane surface, thus the shielding effect will weaken the attraction between hydrophobic sites and contaminants [49]. Although more ALD deposition cycles can bring better hydrophilicity and fouling resistance, the 100-cycle-deposited membranes are more cost-effective and exhibit the best separation performance.

6. Conclusion

In this work, we effectively and quickly functionalize the PTFE HFMs by introducing CFD simulation to optimize the ALD operational parameters. Simulation results show that reaction pressure, fluid flow and active site density are all important for ALD deposition. Increasing reaction pressure and strengthening fluid flow can promote deposition rate, but high pressure and intense fluid flow will cause unwanted inhomogeneous deposition. ALD can deposit uniform Al_2O_3 on substrates with either abundant or scarce active sites, while the number of active sites has significant impact on the deposition rate. Based on simulation results, we have determined the appropriate reaction pressure and deposition location to perform ALD functionalization of PTFE HFMs.

With the deposition of Al_2O_3 on PTFE membrane fibrils, the membrane pore size is narrowing down and the WCA of the membrane is sequentially tuned from hydrophobic to hydrophilic. Through the synergistic effect of the pore reduction and hydrophilization, the trade-off effect between the selectivity and permeability is broken easily after only 1.9 wt% Al_2O_3 (100 cycles) depositing on the PTFE HFMs. The PWP and rejection towards 22-nm SiO_2 microspheres of the membranes increase from ~96 L/(m^2 h bar) and ~77.1% to 188 L/(m^2 h bar) and 93.4%, respectively. The hydrophilic Al_2O_3 also enhances the fouling resistance of the PTFE HFMs, which can reduce up to ~37.5% BSA adsorption on the membrane surface. Overall, with the assistance of CFD simulation, the ALD functionalization of the PTFE HFMs is optimized without tedious experiments. After deposited with tiny amount of Al_2O_3, the separation performances of the PTFE HFMs are significantly enhanced. Comparing with previous ALD based membrane functionalization, the most appealing aspect of this strategy is the ability to significantly reduce the time- and labor-consuming trial-and-error experiments, which are generally used to pursue the optimized ALD parameters. Moreover, CFD will deepen our understanding of interactions between ALD parameters, substrates, and final products, which will accelerate the introduction of ALD into brand-new separation materials and swiftly turn these materials into practical utilization in future.

Author statement

Sen Xiong: Methodology, Data curation, Writing-orginal draft preparation.
Xiaojuan Jia: Investigation, Validation.
Kai Mi: Writing-review & editing.
Yong Wang: Conceptualization, Supervision.
All authors have approved to the final version of the manuscript.

Declaration of competing interest

The authors declare that they have no known competing financial

interests or personal relationships that could have appeared to influence the work reported in this paper.

Acknowledgements

Financial supports from National Key Research and Development Program of China (2018YFE0203502); Jiangsu Natural Science Foundation (BK20190677), National Natural Science Foundation of China (21908096), and Natural Science Foundation of the Higher Education Institutions of Jiangsu Province (19KJB530007) are acknowledged.

Appendix A. Supplementary data

Supplementary data to this article can be found online at https://doi.org/10.1016/j.memsci.2020.118610.

References

[1] J.H. Jhaveri, Z.V.P. Murthy, A comprehensive review on anti-fouling nanocomposite membranes for pressure driven membrane separation processes, Desalination 379 (2016) 137–154.
[2] K.P. Lee, T.C. Arnot, D. Mattia, A review of reverse osmosis membrane materials for desalination-Development to date and future potential, J. Membr. Sci. 370 (1) (2011) 1–22.
[3] W. Pronk, A. Ding, E. Morgenroth, N. Derlon, P. Desmond, M. Burkhardt, B. Wu, A. G. Fane, Gravity-driven membrane filtration for water and wastewater treatment: a review, Water Res. 149 (2019) 553–565.
[4] S. Feng, Z. Zhong, Y. Wang, W. Xing, E. Drioli, Progress and perspectives in PTFE membrane: preparation, modification, and applications, J. Membr. Sci. 549 (2018) 332–349.
[5] S. Wang, J. Li, J. Suo, T. Luo, Surface modification of porous poly (tetrafluoroethylene) film by a simple chemical oxidation treatment, Appl. Surf. Sci. 256 (7) (2010) 2293–2298.
[6] F. Wang, H.L. Zhu, H.P. Zhang, H.Y. Tang, J.Y. Chen, Y.H. Guo, Effect of surface hydrophilic modification on the wettability, surface charge property and separation performance of PTFE membrane, J. Water Process Eng. 8 (2015) 11–18.
[7] M. Kuzuya, T. Yamashiro, S.-i. Kondo, M. Tsuiki, A novel method to introduce durable hydrophilicity onto hydrophobic polymer surface by plasma treatment, Plasma Polym. 2 (2) (1997) 133–142.
[8] J.M. Colwell, E. Wentrup-Byrne, J.M. Bell, L.S. Wielunski, A study of the chemical and physical effects of ion implantation of micro-porous and nonporous PTFE, Surf. Coating. Technol. 168 (2) (2003) 216–222.
[9] S.Y. Park, J.W. Chung, S.-Y. Kwak, Regenerable anti-fouling active PTFE membrane with thermo-reversible “peel-and-stick” hydrophilic layer, J. Membr. Sci. 491 (2015) 1–9.
[10] H.M. Song, H.W. Yu, L.J. Zhu, L.X. Xue, D.C. Wu, H. Chen, Durable hydrophilic surface modification for PTFE hollow fiber membranes, React. Funct. Polym. 114 (2017) 110–117.
[11] C.-L. Lai, R.-M. Liou, S.-H. Chen, G.-W. Huang, K.-R. Lee, Preparation and characterization of plasma-modified PTFE membrane and its application in direct contact membrane distillation, Desalination 267 (2) (2011) 184–192.
[12] Y.J. Qian, L.N. Chi, W.L. Zhou, Z.J. Yu, Z.Z. Zhang, Z.J. Zhang, Z. Jiang, Fabrication of TiO_2-modified polytetrafluoroethylene ultrafiltration membranes via plasma-enhanced surface graft pretreatment, Appl. Surf. Sci. 360 (2016) 749–757.
[13] F. Li, L. Li, X. Liao, Y. Wang, Precise pore size tuning and surface modifications of polymeric membranes using the atomic layer deposition technique, J. Membr. Sci. 385–386 (2011) 1–9.
[14] S.M. George, Atomic layer deposition: an overview, Chem. Rev. 110 (1) (2010) 111–131.
[15] J. Feng, S. Xiong, Y. Wang, Atomic layer deposition of TiO_2 on carbon-nanotube membranes for enhanced capacitive deionization, Separ. Purif. Technol. 213 (2019) 70–77.
[16] J. Feng, S. Xiong, Y. Wang, Atomic layer deposition of hybrid metal oxides on carbon nanotube membranes for photodegradation of dyes, Compos. Commun. 12 (2019) 39–46.
[17] J. Feng, S. Xiong, Z. Wang, Z. Cui, S.-P. Sun, Y. Wang, Atomic layer deposition of metal oxides on carbon nanotube fabrics for robust, hydrophilic ultrafiltration membranes, J. Membr. Sci. 550 (2018) 246–253.
[18] D. Li, J. Hu, Z.-X. Low, Z. Zhong, Y. Wang, Hydrophilic ePTFE membranes with highly enhanced water permeability and improved efficiency for multipollutant control, Ind. Eng. Chem. Res. 55 (10) (2016) 2806–2812.
[19] M. Weber, A. Julbe, A. Ayral, P. Miele, M. Bechelany, Atomic layer deposition for membranes: basics, challenges, and opportunities, Chem. Mater. 30 (21) (2018) 7368–7390.
[20] H.-C. Yang, R.Z. Waldman, Z. Chen, S.B. Darling, Atomic layer deposition for membrane interface engineering, Nanoscale 10 (44) (2018) 20505–20513.
[21] S.-L. Wu, F. Liu, H.-C. Yang, S.B. Darling, Recent progress in molecular engineering to tailor organic–inorganic interfaces in composite membranes, Mol. Syst. Des. Eng. 5 (2) (2020) 433–444.
[22] Q. Xu, Y. Yang, X.Z. Wang, Z.H. Wang, W.Q. Jin, J. Huang, Y. Wang, Atomic layer deposition of alumina on porous polytetrafluoroethylene membranes for enhanced hydrophilicity and separation performances, J. Membr. Sci. 415–416 (2012) 435–443.
[23] S. Xiong, L. Kong, Z. Zhong, Y. Wang, Dye adsorption on zinc oxide nanoparticulates atomic-layer-deposited on polytetrafluoroethylene membranes, AIChE J. 62 (11) (2016) 3982–3991.
[24] Q. Wang, X. Wang, Z. Wang, J. Huang, Y. Wang, PVDF membranes with simultaneously enhanced permeability and selectivity by breaking the tradeoff effect via atomic layer deposition of TiO_2, J. Membr. Sci. 442 (2013) 57–64.
[25] S. Xiong, Y. Yang, Z. Zhong, Y. Wang, One-step synthesis of carbon-hybridized ZnO on polymeric foams by atomic layer deposition for efficient absorption of oils from water, Ind. Eng. Chem. Res. 57 (4) (2018) 1269–1276.
[26] T. Turken, R. Sengur-Tasdemir, E. Ates-Genceli, V.V. Tarabara, I. Koyuncu, Progress on reinforced braided hollow fiber membranes in separation technologies: a review, J. Water Process Eng. 32 (2019) 100938.
[27] X. Jia, Z. Low, H. Chen, S. Xiong, Y. Wang, Atomic layer deposition of Al_2O_3 on porous polypropylene hollow fibers for enhanced membrane performances, Chin. J. Chem. Eng. 26 (4) (2018) 695–700.
[28] M.B.M. Mousa, C.J. Oldham, J.S. Jur, G.N. Parsons, Effect of temperature and gas velocity on growth per cycle during Al_2O_3 and ZnO atomic layer deposition at atmospheric pressure, J. Vac. Sci. Technol. 30 (1) (2012), 01A155.
[29] J.S. Jur, G.N. Parsons, Atomic layer deposition of Al_2O_3 and ZnO at atmospheric pressure in a flow tube reactor, ACS Appl. Mater. Interfaces 3 (2) (2011) 299–308.
[30] M.R. Shaeri, T.-C. Jen, C.Y. Yuan, Improving atomic layer deposition process through reactor scale simulation, Int. J. Heat Mass Tran. 78 (2014) 1243–1253.
[31] D. Pan, L. Ma, Y. Xie, T.C. Jen, C. Yuan, On the physical and chemical details of alumina atomic layer deposition: a combined experimental and numerical approach, J. Vac. Sci. Technol. 33 (2) (2015), 021511.
[32] Z. Deng, W. He, C. Duan, B. Shan, R. Chen, Atomic layer deposition process optimization by computational fluid dynamics, Vacuum 123 (2016) 103–110.
[33] H.F. Barton, A.K. Davis, G.N. Parsons, The effect of surface hydroxylation on MOF formation on ALD metal oxides: MOF-525 on TiO_2/polypropylene for catalytic hydrolysis of chemical warfare agent simulants, ACS Appl. Mater. Interfaces 12 (13) (2020) 14690–14701.
[34] D. Pan, T. Li, T.C. Jen, C. Yuan, Numerical modeling of carrier gas flow in atomic layer deposition vacuum reactor: a comparative study of lattice Boltzmann models, J. Vac. Sci. Technol. 32 (1) (2014), 01A110.
[35] Y. Zhang, Y. Ding, P.D. Christofides, Multiscale computational fluid dynamics modeling of thermal atomic layer deposition with application to chamber design, Chem. Eng. Res. Des. 147 (2019) 529–544.
[36] S.-M. Lee, V. Ischenko, E. Pippel, A. Masic, O. Moutanabbir, P. Fratzl, M. Knez, An alternative route towards metal–polymer hybrid materials prepared by vapor-phase processing, Adv. Funct. Mater. 21 (16) (2011) 3047–3055.
[37] C.A. Wilson, R.K. Grubbs, S.M. George, Nucleation and growth during Al_2O_3 atomic layer deposition on polymers, Chem. Mater. 17 (23) (2005) 5625–5634.
[38] G.N. Parsons, J.W. Elam, S.M. George, S. Haukka, H. Jeon, W.M.M. Kessels, M. Leskelä, P. Poodt, M. Ritala, S.M. Rossnagel, History of atomic layer deposition and its relationship with the American Vacuum Society, J. Vac. Sci. Technol. 31 (5) (2013), 050818.
[39] Q. Xu, Y. Yang, J. Yang, X. Wang, Z. Wang, Y. Wang, Plasma activation of porous polytetrafluoroethylene membranes for superior hydrophilicity and separation performances via atomic layer deposition of TiO_2, J. Membr. Sci. 443 (2013) 62–68.
[40] X. Yang, P. Sun, H. Zhang, Z. Xia, R.Z. Waldman, A.U. Mane, J.W. Elam, L. Shao, S. B. Darling, Polyphenol-sensitized atomic layer deposition for membrane interface hydrophilization, Adv. Funct. Mater. 30 (15) (2020) 1910062.
[41] G.C. Liu, C.J. Gao, X.M. Li, C.G. Guo, Y. Chen, J.L. Lv, Preparation and properties of porous polytetrafluoroethylene hollow fiber membrane through mechanical operations, J. Appl. Polym. Sci. 132 (43) (2015).
[42] S. Xiong, L. Kong, Z.X. Zhong, Y. Wang, Dye adsorption on zinc oxide nanoparticulates atomic-layer-deposited on polytetrafluoroethylene membranes, AIChE J. 62 (11) (2016) 3982–3991.
[43] R.Z. Waldman, H.-C. Yang, D.J. Mandia, P.F. Nealey, J.W. Elam, S.B. Darling, Janus membranes via diffusion-controlled atomic layer deposition, Adv. Mater. Interfaces 5 (15) (2018) 1800658.
[44] Q. Lan, Y. Wang, Carbonization of gradient phenolics filled in macroporous substrates for high-flux tight membranes: toward ultrafiltration of polypeptides, J. Membr. Sci. 590 (2019) 117309.
[45] B.M. Ganesh, A.M. Isloor, A.F. Ismail, Enhanced hydrophilicity and salt rejection study of graphene oxide-polysulfone mixed matrix membrane, Desalination 313 (2013) 199–207.
[46] J.H. Feng, S. Xiong, Z.G. Wang, Z.L. Cui, S.P. Sun, Y. Wang, Atomic layer deposition of metal oxides on carbon nanotube fabrics for robust, hydrophilic ultrafiltration membranes, J. Membr. Sci. 550 (2018) 246–253.
[47] F. Xu, M. Wei, X. Zhang, Y. Song, W. Zhou, Y. Wang, How pore hydrophilicity influences water permeability? Research 2019 (2019) 10.
[48] F. Yalcinkaya, A. Siekierka, M. Bryjak, Preparation of fouling-resistant nanofibrous composite membranes for separation of oily wastewater, Polymers 9 (12) (2017) 679.
[49] H.-C. Yang, Y. Xie, H. Chan, B. Narayanan, L. Chen, R.Z. Waldman, S.K.R. S. Sankaranarayanan, J.W. Elam, S.B. Darling, Crude-oil-repellent membranes by atomic layer deposition: oxide interface engineering, ACS Nano 12 (8) (2018) 8678–8685.